International Symposium
On Turbulence and Shear Flow
Phenomena (TSFP-9)
June 30 - July 3, 2015 *Melbourne, Australia*

SPATIALLY DEVELOPING LAMINAR MIXING LAYER FORCED BY VELOCITY AND THERMAL PERTURBATIONS DOWNSTREAM OF A SPLITTER PLATE

Z. L. Chen, B. Q. Zhang
Institute of Fluid Mechanics
Northwestern Polytechnical University
Youyi Xilu 127 Xi'an, Shaanxi, 710072, China
zhenlichen,bqzhang@nwpu.edu.cn

S. Hickel, N. A. Adams
Institute of Aerodynamics and Fluid Mechanics
Technische Universität München
Boltzmannstr. 15, D-85748 Garching b. München, Germany
sh,nikolaus.adams@tum.de

ABSTRACT

In this work our first objective is to study the spatial development of a laminar compressible mixing layer after a splitter plate at relatively high Reynolds number by using an implicit large-eddy simulation. A blowing and suction strip is used on the upper wall of the plate to promote the shear layer instability. In the perspective of flow control our second objective is to understand the effects of a strong thermal forcing to modify the spatial development. In the momentum-forcing case three distinct flow regions exists: a linear instability region, a mixing-transition region and a fully developed turbulent region, which has much different vorticity growth rate. In the fully developed region the distributions of mean velocity collapse into a self-similar profile. There is no spanwise roller observed near the trailing edge of the plate. When the thermal forcing is also applied, it introduces two-dimensional spanwise rollers. Two successive spanwise roller pairing are observed. The vorticity thickness and its growth rate are totaly different. At the end of the simulation domain the flow is not fully turbulent. Different Mach wave radiations are observed in the fast stream. Therefore, the thermal forcing can effectively to modify the spatial development of the mixing layer.

INTRODUCTION

As the plane mixing layer is of fundamental importance to understand the turbulence and mixing, and is of great technological relevance to practical devices, there were large amount of experiments and numerical simulations, since the observation of large coherent structures in the experiments of Brown and Roshko Brown & Roshko (1974). There are still some unanswered questions, as what are the effects of the trailing edge of a splitter plate and the mechanisms of the development of small-scale, three-dimensional motions (mixing transition) finally to turbulence. Recently, highly resolved DNSs of spatially developing mixing layers with the splitter plate trailing edge had been carried out. Splitter plate with three different trailing edges were used to investigate the effects of their wakes Laizet *et al.* (2010). It was shown that the wake of splitter plate plays a very dominant role in the development of the flow and strongly interacts with the mixing layer, which is consistent with the experiments of Mehta Mehta (1991).

Direct Numerical Simulation (DNS) is a powerful tool that can be used to simulate the detail development of the mixing layer. However, it is limited to temporal or spatial simulations at relatively low Reynolds number Rogers & Moser (1992, 1994); Sandham & Sandberg (2009), due to computational expense. Furthermore, none of the temporal simulations is able to take into account the presence of the splitter plate in the experiments.

In this work our first objective is to study the spatial development of a laminar compressible mixing layer after a splitter plate at relatively high Reynolds number by using an implicit large-eddy simulation (LES) method. The implicit LES adopts the Adaptive Local Deconvolotion Method (ALDM) Hickel *et al.* (2014). In order to avoid an arbitrary perturbation, a blowing and suction strip is used on the upper wall of the plate.

The sensitivity of the mixing layer to upstream influences is not limited to the state of the boundary layers separating from the splitter plate. Numerous experiments and simulations Bell & Mehta (1990); Attili & Bisetti (2012) have shown that the disturbances introduced near the origin of the mixing layer can produce very different flow development far downstream. In the perspective of flow control, this disturbance-dependent characteristic can be very useful. It is expected to utilize certain disturbances to promote intrinsic instability of the base flow to realize flow control objectives. Therefore, our second objective is to understand the effects of a strong thermal forcing introduced upstream of the blowing and suction strip to modify the downstream development of the mixing layer. The thermal forcing resembles the effect of a nanosecond pulsed dielectric barrier discharge Roupassov *et al.* (2009) utilized in flow control.

NUMERICAL METHODS

Governing Equations

The unsteady compressible Navier-Stokes equations in conservative form are used to describe the gas dynamics, which are written as:

$$\partial_t \mathbf{U} + \nabla \cdot \mathbf{F}(\mathbf{U}) + \nabla \cdot \mathbf{D}(\mathbf{U}) = \mathbf{S}, \tag{1}$$

with the solution vector $\mathbf{U} = [\rho, \rho u_1, \rho u_2, \rho u_3, E]^T$. The conserved variables are density ρ, momentum ρu_i and total energy $E = \rho e + 0.5\rho u_i u_i$. The convective flux is

$$\mathbf{F}_i(\mathbf{U}) = [u_i\rho, u_i\rho u_1 + \delta_{i1}p, u_i\rho u_2 + \delta_{i2}p, u_i\rho u_3 + \delta_{i3}p, u_i(E+p)]^T, \tag{2}$$

and the diffusive flux is

$$\mathbf{D}_i(\mathbf{U}) = [0, -\tau_{i1}, -\tau_{i2}, -\tau_{i3}, -u_k\tau_{ik} + q_i]^T, \tag{3}$$

where u_i is the velocity vector, τ_{ij} are the components of the viscous stress tensor

$$\tau_{ij} = \mu(T)(\partial_j u_i + \partial_i u_j - 2/3\delta_{ij}\partial_k u_k), \tag{4}$$

and the heat flux is

$$q_i = -\kappa\partial_i T. \tag{5}$$

The transport properties, dynamic viscosity μ and thermal conductivity κ depend on temperature T. They are calculated as

$$\mu(T) = \mu_\infty(\frac{T}{T_\infty})^{2/3},\ \kappa = \frac{\mu c_p}{Pr}, \tag{6}$$

where μ_∞ and T_∞ are the freestream dynamic viscosity and temperature. $c_p = \gamma R/(\gamma - 1)$ is the heat capacity at constant pressure with $\gamma = 1.4$ and gasconstant $R = 287.15(J/kg \cdot K)$. A constant Prandtl number $Pr = 0.72$ for the air is used. To close the system of equations the pressure p is related to density ρ and temperature T by the equation of state

$$p = \rho RT. \tag{7}$$

The governing equations are nondimensionalized by the velocity difference ΔU of the fast-stream velocity U_1 and the slow-stream velocity U_2, the density ρ_1 and temperature T_1 of the fast stream and the vorticity thickness δ_{ω_0} of the mixing layer at the end of the splitter plate. The pressure is nondimensionalized using $\rho_1 \triangle U^2$. The nondimensional flow parameters are the Reynolds number $Re_{\delta_{\omega_0}} = \rho_1 \Delta U \delta_{\omega_0}/\mu_1 = 877$ and the Mach number $Ma = \Delta U/a_1$, where μ_1 and a_1 are the viscosity and the speed of sound of the fast steam, respectively. The ALDM is used to reconstruct the flow variables from the cell-averaged values at the cell interfaces for the convective flux calculation Hickel *et al.* (2014). A flux vector splitting method based on the characteristic decomposition of the Jacobian matrixes for the nonlinear convective terms is used to calculate the fluxes at cell interfaces. A second-order central scheme is used to discretize the diffusive terms. An explicit third order TVD Rulnge-Kutta method is used for time advancement.

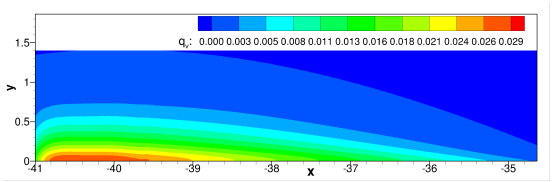

Figure 1. Power density distribution of the thermal forcing.

Simulation Setup

The fast and slow streams of the mixing layer have Mach number $Ma_1 = 0.9$ and $Ma_2 = 0.18$, respectively, at the same temperature and density, which results in a velocity ratio $U_2/U_1 = 0.2$. The two streams are separated by an infinitely thin splitter plate, which has a length of $110\delta_{\omega_0}$.

The simulation domain has a size of $L_x \times L_y \times L_z = 878 \times 550 \times 41$ with a resolution $1152 \times 384 \times 64$ in streamwise, vertical and spanwise directions, respectively. In the vertical direction the grids are stretched near the splitter plate at $y = 0$ to resolve the high shear region. In the streamwise direction the grids are homogeneous from $x = -110$ to $x = 494$ and are stretched to $x = 494$ from the rest part of the domian to eliminate the effect of the outflow boundary condition. On both surfaces of the plate, the flow is initialized by the compressible Blasius solutions. The compressible Blasius solutions are fixed at the inflow with Reynolds number $Re_x = 5 \times 10^4$. The characteristic boundary conditions are applied at the upper, lower boundaries and the outflow. At the inflow, outflow, upper and lower boundaries sponge zones are used to damp boundary reflections. Periodic boundary conditions are applied in the spanwise direction.

The wall-normal velocity perturbation starts at $x_{MF} = -13.7$ on the upper surface and has a wave length $\lambda_x = 6.8$, which is prescribed by a blowing and suction boundary condition of Huai et. al Huai *et al.* (1997)

$$v(x,z,t) = A_1 f(x) sin(\omega_{MF1} t) + A_{1/2} f(x) g(z) sin(\omega_{MF2} t), \tag{8}$$

where, $\omega_{MF1} = \omega_{MF2} = 0.0177$ are the frequencies of the two-dimensional Tollmien-Schlichting and the oblique waves, respectively. $A_1 = 0.0003$ and $A_{1/2} = 1.5 \times 10^{-5}$ are the disturbance amplitudes of the two-dimensional and the oblique waves. $f(x)$ is defined following Fasel & Konzelmann (1990), and $g(z) = cos(2\pi z/\lambda_z)$ with $\lambda_z = 8.2$.

The thermal forcing is realized by using a source term $\mathbf{S} = [0, 0, 0, 0, q_v]^T$. The power density q_v is taken as the thermal effect of a nanosecond pulsed dielectric barrier discharge plasma actuator by an inhomogeneous phenomenological plasma model Chen *et al.* (2013), which is a function of (x, y) positions, as shown in Fig. 1. It is homogeneous in the spanwise direction. The thermal forcing starts at $x_{TF} = -41$ and have a length 6.8 and a maximum height of 1.4, which is upstream of the strip. The maximum magnitude of the forcing is 0.029, which is strong enough to produce a compression wave. The thermal forcing acts on with time 0.033 per pulse at repetitive angular frequency $\omega_{TF} = 0.133$. Hereafter, the "MF" and "TF" represent momentum forcing and thermal forcing, respectively.

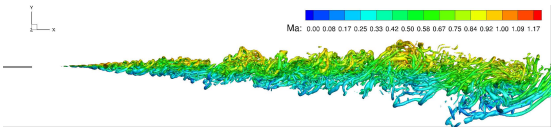

(a) Top view

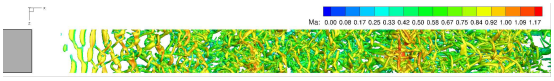

(b) Side View

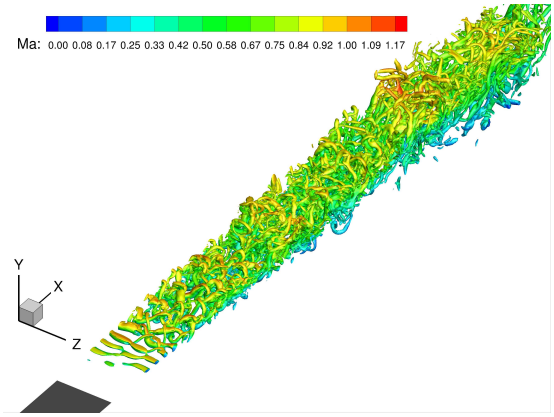

(c) Inclined View

Figure 2. Coherent structures indicated by $\lambda_2 = -0.5$ of the mixing layer with the momentum forcing.

RESULTS AND DISCUSSIONS

First, the weak momentum forcing is applied. The simulation is performed for 5 times flow-through time and then the statistics are carried out for 45 times flow-through time until the statistics converge. In the thermal forcing case, after the flow well developed with momentum forcing, the thermal forcing is also applied upstream the strip. The effects of the splitter plate and the thermal forcing will be analyzed in detail as in the following.

Momentum Forcing

The coherent structures indicated by $\lambda_2 = -0.5$ are shown in Fig. 2 from top, side and inclined views. There are no obvious two-dimensional spanwise rollers but inclined coherent structures observed, which is similar with the spatial DNS results of Laizet *et al.* (2010) and Wang *et al.* (2007). Between the inclined vortices longitudinal vortices gradually form and develop into hairpin vortices. These large hairpin vortices continue to exist at the edges of the free shear layer, whereas small structures form in the shear layer, as shown in Fig.2(c). At certain streamwise positions, the local Mach number is supersonic, which is corresponding to the top of the large structures.

In order to know the effects of these supersonic regions, a numerical Schlieren image of the $z = 20.5$ plane at the same time with the coherent structures is shown in Fig.3. On the top of the spanwise structures, three compression waves are obvious. These waves move very slowly upstream but do not go along with spanwise structures in the time-series Schlieren motivation. This Mach wave radiation can be attributed to that the velocity difference between the

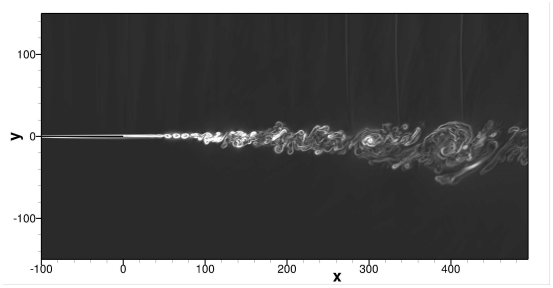

Figure 3. Instantaneous computational Schlieren image at $z = 20.5$ in the momentum forcing case.

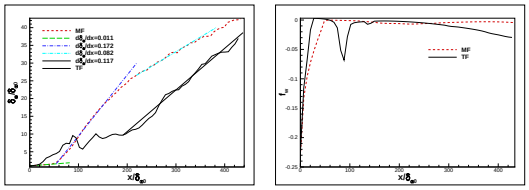

(a) Vorticity thickness (b) Wake effect parameter

Figure 4. Comparison of velocity defect parameter and vorticity thickness for momentum and both forcing cases.

convection velocity of large-scale structures and that of the fast stream is greater than the local speed of sound.

The vorticity thickness is of great importance to characterize the mixing layer. It has three distinct growth rates0.011, 0.172 and 0.082, as shown in Fig. 4(a). Downstream of the trailing edge the mixing layer grows linearly and very slowly till $x \simeq 48$. Then the mixing layer grows linearly and much fast till $x \simeq 156$. Finally, the growth rate gradually decreases and approaches an asymptotic value. These different growth rates can be attributed to three developing stages: linear instability, nonlinear mixing transition and highly three-dimensional turbulence, which can be verified from the streamwsie development of the coherent structures in Fig.2 and from the instantaneous computational Schlieren image in Fig.3.

To verify that the mixing layer has well developed into turbulence, the streamwise velocity spectra is compared in Fig.5 at the mixing-layer center of different streamwise positions. In the linear instability region at $x = 27$, the power spectra density is lower and has no inertial region. Spectra peak at $\omega \simeq = 0.4$ and its harmonics at high frequencies can be observed. However, this frequency is not corresponding to the forcing frequency, which means that the flow instability is not directly promoted by the momentum forcing. In the transition region at $x = 110$, the energy containing structures at lower frequency appear but there is still no inertial region. At $x = 220$ the spectra has a lower frequency energy containing region, an inertial region with slope $-5/3$ and a high frequency dissipation regio, which indicates the flow has well developed into turbulence.

A velocity defect parameter $f_w = (U_{min} - U_2)/\Delta U$ is defined as in the experiment of Mehta (1991) to exhibit the wake effect, which is shown in Fig. 4(b). The wake effect is large till $x \simeq 50$. This may lead to the small growth rate of the vorticity thickness from the end of the splitting plate to this position. After that position the value of f_w is not exactly zero, as the minimum velocity at the lower computational

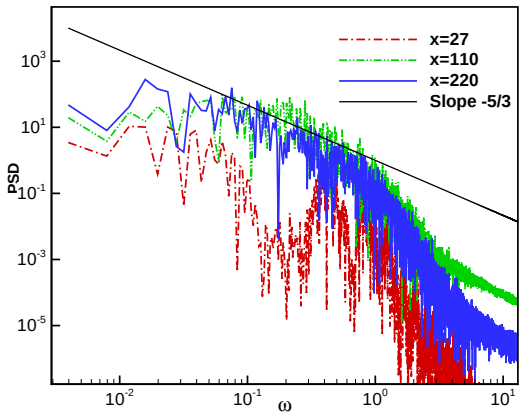

Figure 5. Comparisons of power spectra density for streamwise velocity at three streamwise positions.

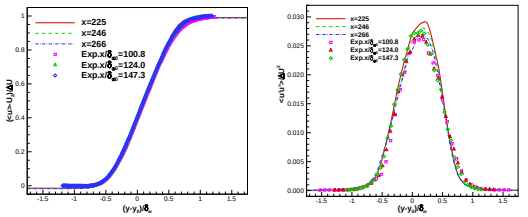

(a) Mean velocity (b) Streamwise Reynolds stress

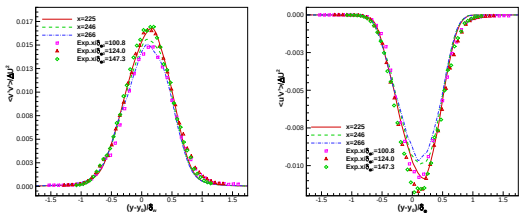

(c) Vertical Reynolds stress (d) Reynolds shear stress

Figure 6. Comparisons of computational and experimental mean velocity and Reynolds stresses.

domain does not reach at the exact freestream velocity U_2.

In the fully developed region, the mean streamwise velocity and Reynolds stresses are compared with the incompressible experimental data of Delville (1995), as shown in Fig. 6. The mean velocity profiles reach self-similar state and coincide well with the experimental data. However, near the upper edge of the mixing layer the mean velocity profile has larger gradient than the experimental data, which may be attributed to the compressibility effect of the upper stream. The Reynolds stresses are also well predicted. As the experimental data the maximum Reynolds stresses do not collapse well at different streamwise positions.

Momentum and Thermal Forcing

When the strong thermal forcing is also applied upstream of the blowing and suction strip, the spatial development of the mixing layer changes totally different, as indicated by the coherent structures shown in Fig. 7. As the

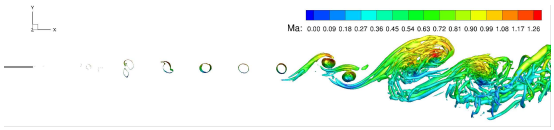

(a) Top view

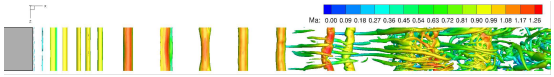

(b) Side View

Figure 7. Coherent structures indicated by $\lambda_2 = -0.5$ of the mixing layer with momentum and thermal forcing.

thermal forcing is two dimensional and is much strong than the momentum forcing, two dimensional spanwise rollers form very fast near the trailing edge of the splitter plate under the combined forcing. It can be suspected that the effect of momentum forcing is suppressed or overrode by the thermal forcing. At streamwise position $x = 90$ the first paring of the spanwise rollers appears almost at this fixed streamwise position. Then larger spanwise roller forms and the second roller pairing appears at $x \simeq 290$, however, the second pairing position is not fixed but oscillates with time in the streamwise direction. Just before the second paring the rib vortices develop in the braid region. After second pairing position the rib vortices become stronger. No single spanwise roller is obvious but small structures appear near the core region due to the core instability. The flow is not fully turbulent at the end of the effective simulation domain.

The formation frequency of the two dimensional spanwise rollers is the same as the thermal forcing frequency $\omega_{TF} = 0.133$, as indicated by the power spectra density at $x = 17$, shown in Fig. 8(a). At this position spectra peaks appear at the thermal-forcing frequency harmonics till very high frequency. At $x = 110$ the first and second harmonics still contain almost the same energy as at $x = 17$. Large energy-containing structures appear at low frequency. However, the higher frequency harmonics are damped. At $x = 220$ the spectra peak at forcing frequency can still be observed with its subharmonic and first harmonic, but no obvious inertial region exists even at far downstream at $x = 274$.

It deserves to note that under the combined forcing the maximum local Mach number $Ma = 1.26$ is much larger than that under the momentum forcing, comparing Fig. 7 and Fig. 2. The local Mach number is noticeably large at the first and second pairing positions. As expected, stronger Mach wave radiation can be observed in the numerical Schlieren image, as shown in Fig. 9. The thermal forcing is so strong that a compression wave is produced for each actuation. Note that the two-dimensional compression wave scatters around the trailing edge, which may trigger two-dimensional vortical modes as analysed by Sandham & Sandberg (2009). However, in our former investigation the vorticity source introduced by the thermal forcing is due to a baroclinic effect Chen *et al.* (2014). Twice pairings can also be clearly observed in the Schlieren image.

As the consequence of the spatial development under the combined forcing, the vorticity thickness also changes a lot, as shown in Fig. 4(a). Upstream $x \simeq 20$ the growth rate of the vorticity thickness is almost the same under the momentum forcing and the combined forcing. Downstream

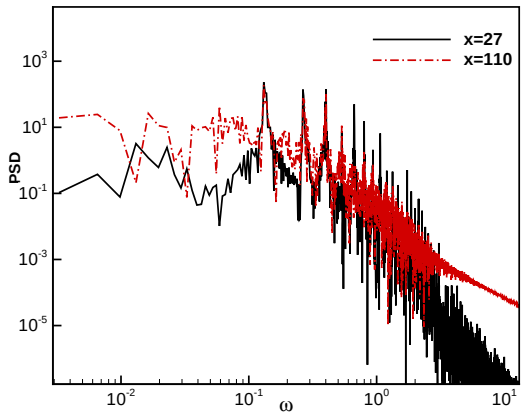

(a) Power spectra density at $x = 17$ and $x = 110$

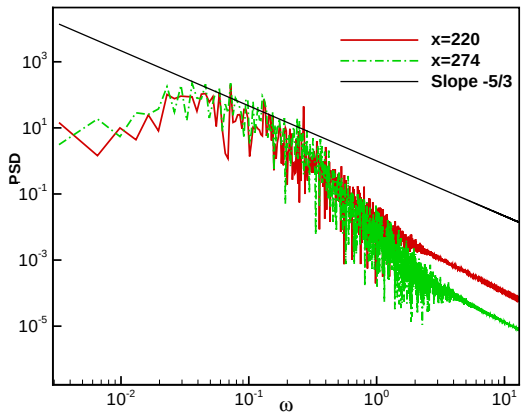

(b) Power spectra density at $x = 220$ and $x = 274$

Figure 8. Comparisons of power spectra density for streamwise velocity at four streamwise positions.

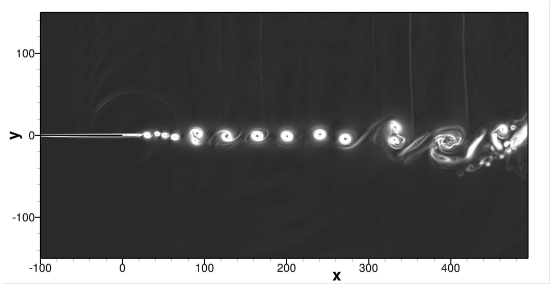

Figure 9. Instantaneous computational Schlieren image at $z = 20.5$ in the momentum and thermal forcing case.

that position the growth rate and the vorticity thickness of the combined forcing case are much larger than those of the momentum forcing case before the first pairing position. After that the vorticity thickness suddenly decreases due to pairing, but the growth rate has a mean value of 0.117. Due to the lack of the transition region with high growth rate as in the momentum forcing case, the vorticity thickness becomes much small from the first paring position to the end of the simulation domain.

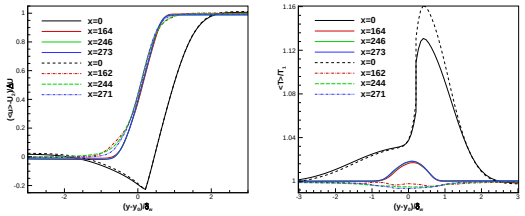

(a) Mean streamwise velocity (b) Mean temperature

Figure 10. Comparisons of mean streamwise velocity and temperature in the momentum and both forcing cases at different streamwise positions.

A large wake effect can still be observed till $x = 20$, but it is smaller and shorter than in the momentum forcing case, as compared in Fig. 4(b). It is obvious that the small growth rate of momentum thickness is corresponding to the large wake effect region in both cases. The value of f_w is small near the pairing position.

The mean streamwise velocity and temperature are compared with those in the momentum-forcing case in Fig. 10. At the end of the splitter plate the mean velocity has very small difference, which means the additional thermal forcing almost does not change the mean velocity of the boundary layer. However, the mean temperature increases due to thermal forcing in the upper stream near the wall, as shown in Fig. 10(b). At downstream positions the mean velocity does not reach self-similar state as in the momentum forcing case. The mean temperature in the shear layer is lower than the free-stream temperature, which can be attributed to the large fluctuation temperature, as shown in Fig. 12(a). In the momentum forcing case the mean temperature distribution also approaches a self-similar profile.

The Reynolds stresses components $< u'u' >$, $< v'v' >$ and $< u'v' >$ in the combined forcing case are much larger than those in the momentum forcing case, as compared in Fig. 11. At $x = 162$ even far from the first pairing position, the streamwise Reynolds stress still exhibits two peaks. The vertical and shear components have no this characteristics. The component $< w'w' >$ is much smaller due to its two-dimensional flow structures, especially at $x = 162$.

As the thermal forcing introduce perturbations to temperature, density and pressure, the autocorrelation of fluctuation temperature and fluctuation density are given in Fig. 12. The fluctuation of thermal variables are much smaller than the velocity fluctuation. In the momentum forcing case the autocorrelations of fluctuation temperature and density collapse well at $x = 264$ and $x = 273$. However, in the combined forcing case they have large variations.

CONCLUSIONS

The effects of different forcing on the spatial development of a laminar compressible mixing layer after a splitter plate is studied by using an implicit LES method. A momentum and a thermal forcing are applied.

In the momentum-forcing case three distinct regions exists: a linear instability region, a mixing-transition region and a fully developed turbulent region, which has much different vorticity growth rate. In the fully developed region the distributions of mean velocity collapse into a self-

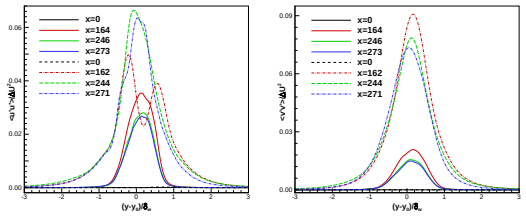

(a) Streamwise Reynolds stress (b) Vertical Reynolds stress

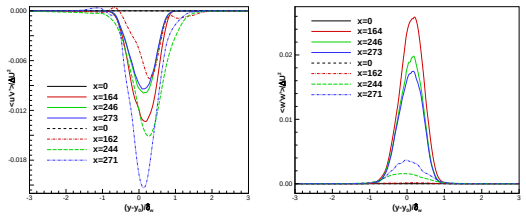

(c) Reynolds shear stress (d) Spanwise Reynolds stress

Figure 11. Comparisons of Reynolds stresses in the momentum and both forcing cases.

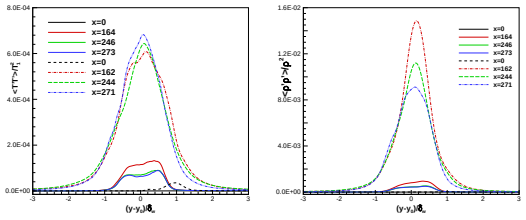

(a) Autocorrelation of temperature fluctuation (b) Autocorrelation of density fluctuation

Figure 12. Comparisons of mean temperature and density fluctuation square in the momentum and both forcing cases at different streamwise positions.

similar profile. There is no spanwise roller observed near the trailing edge of the plate, but rib vortices are observed in the mixing transition region. The hairpin vortices appear at the edges of the mixing layer from the mixing-transition region to the fully developed region. Corresponding to the top of the large structures the local Mach number is supersonic, which results in Mach wave radiation in the fast stream.

When the thermal forcing is also applied, it suppresses the momentum forcing and introduces two-dimensional spanwise rollers having the same frequency as the thermal forcing. Two successive spanwise roller pairing are observed. The vorticity thickness is larger than that in the momentum forcing case near the plate trailing edge, but it is much small after the first paring position. At the end of the simulation domain the flow is not fully turbulent. The velocity and thermal fluctuations are large than that in the momentum-forcing case except the spanwise velocity fluctuation. The stronger Mach wave radiations are also observed near the two pairing positions. Therefore, in the perspective of flow control, the thermal forcing can effectively to modify the spatial development of the mixing layer.

ACKNOWLEDGMENT

This work is founded by National Natural Science Foundation of China under contract No. 11402211.

REFERENCES

Attili, A & Bisetti, F. 2012 Statistics and scaling of turbulence in a spatially developing mixing layer at $re_\lambda = 250$. *Phys. Fluids* **24**, 1035109.

Bell, J. H. & Mehta, R. D. 1990 Development of a two-stream mixing layer from tripped and untripped boundary layers. *AIAA J.* **28**, 2034–2042.

Brown, G. L. & Roshko, A. 1974 On density effects and large structure in the turbulent mixing layers. *J. Fluid Mech.* **64**, 775–816.

Chen, Z. L., Hao, L. Z. & Zhang, B. Q. 2013 A model for nanosecond pulsed dielectric barrier discharge NSDBD actuator and its investigation on the mechanisms of separation control over an airfoil. *Sci. China Tech. Sci.* **56(5)**, 1055–1065.

Chen, Z. L., Zhang, S., Zhang, B. Q. & Ma, J. 2014 Shock-induced separation control by using nanosecond pulsed sdbd plasma actuators. *AIAA paper 2014-2368* .

Delville, J. 1995 La décomposition orthogonale aux valeurs propres et l'analyse de l'organisation tridimensionnelle des écoulements turbulents cisaillés libres. PhD thesis, Université de Poitiers.

Fasel, H. & Konzelmann, U. 1990 Non-parallel stability of a flat-plate boundary layer using the complete navier-stokes equations. *J. Fluid Mech.* **221**, 311–347.

Hickel, S., Egerer, C. P. & Larsson, J. 2014 Subgrid-scale modeling for implicit large eddy simulation of compressible flows and shock-turbulence interaction. *Phys. Fluids* **26**, 106101.

Huai, X., Joslin, R. D. & Piomelli, U. 1997 Large-eddy simulation of transition to turbulence in boundary layers. *Theor. Comput. Fluid Dyn.* **9**, 149–163.

Laizet, S., Lardeau, S. & Lamballais, E. 2010 Direct numerical simulation of a mixing layer downstream a thick splitter plate. *Phys. Fluids* **22**, 015104.

Mehta, R. D. 1991 Effect of velocity ratio on plane mixing layer development: Influence of the splitter plate wake. *Exp. Fluids* **10**, 194–204.

Rogers, M. M. & Moser, R. D. 1992 The three-dimensional evolution of a plane mixing layer: the kelvin-helmoltz roll-up. *J. Fluid Mech.* **243**, 183–226.

Rogers, M. M. & Moser, R. D. 1994 Direct simulation of a self-similar turbulent mixing layer. *Phys. Fluids* **6**, 903–922.

Roupassov, D. V., Nikipelov, A. A., Nudnova, M. M. & Starikovskii, A. Yu. 2009 Flow separation control by plasma actuator with nanosecond pulsed-periodic discharges. *AIAA J.* **47**, 168.

Sandham, N. D. & Sandberg, R. D. 2009 Direct numerical simulation of the early development of a turbulent mixing layer downstream of a splitter plate. *J. Turbul.* **10**, 1–17.

Wang, Y., Tanahashi, M. & Miyauchi, T. 2007 Coherent fine scale eddies in turbulence transition of spatially-developing mixing layer. *Int. J. Heat Fluid Flow* **28**, 1280–1290.